Effect of Energy Distribution on Sorption Kinetics in Bidispersed Particles

Xijun Hu, Gade N. Rao, and Duong D. Do
Dept. of Chemical Engineering, University of Queensland, Brisbane, Queensland 4072, Australia

In this article, we present a model to describe sorption kinetics of gaseous adsorbates onto bidispersed heterogeneous microporous particles. This model describes adsorption and desorption of gaseous adsorbates with allowance for the energy distribution of adsorption site for both equilibrium isotherm and diffusion of the adsorbed species. The adsorbed species of all energy level diffuse in two directions inside the particle. One direction is the direction along the particle coordinate while the other is the direction perpendicular to the particle coordinate (that is, the direction into the grain of the solid). This model is more fundamental than models previously proposed by Do and coworkers. Effects of energy distribution on the adsorption and desorption dynamics are investigated. Extensive experimental analysis of adsorption and desorption dynamics of ethane and propane onto Ajax activated carbon are carried out to validate this theory.

Introduction

Since the mass transfer inside a porous adsorbent is often the controlling resistance in the separation and purification of gases by adsorption technique, its information is essential in the dynamic study and design purposes. Because both pore and surface diffusions are controlling this mass-transfer process in many cases, a lot of published work employing the pore and surface diffusion model have appeared in the literature. Most of them assumed a constant surface diffusivity (Schneider and Smith, 1968; Do, 1983; Ruthven, 1984; Do and Rice, 1987; Bhatia, 1988, Schork and Fair, 1988). The concentration dependent surface diffusion were considered by Doong and Yang (1986), Sun and Meunier (1987), Kapoor and Yang (1991), Do et al., 1991, Hu and Do (1992a). Some researchers also took into account the energetically heterogeneous surfaces, that is, the surface diffusivity is related to the adsorption isotherm through some form of adsorbate-adsorbent interaction energy distribution (Zgrablich et al., 1986; Horas et al., 1988; Seidel and Carl, 1989; Kapoor and Yang, 1989, 1990; Do and Hu, 1992).

However, the previously published diffusion models, either ignore the micropore resistance which is important in small and medium sized particles, or neglect the surface diffusion along the particle coordinate. Recently, Do and co-workers proposed a model including the macropore, surface and micropore diffusions with a constant surface diffusivity (Gray and Do, 1990; Mayfield and Do, 1991) or with a Darken type concentration-dependent surface diffusivity (Hu and Do, 1992b) without the allowance for energy distribution for sorption kinetics.

In this article, we present a model to describe the uptake rate in a heterogeneous microporous particle of any size, taking into account the diffusions in both the gas phase and the adsorbed phase, with the diffusion of the adsorbed phase occurring in two directions. One is the direction along the particle coordinate and the other is the direction into the grain of the solid (microparticle). The heterogeneous surface diffusion is allowed for in both directions. The local diffusion flux of the adsorbed species inside the microparticle is calculated with an aid of an imaginary gas phase concentration concept (Hu and Do, 1992b). Experimental data of two light hydrocarbons—ethane and propane in Ajax activated carbon of different temperatures, concentrations, particle sizes and sorption modes (adsorption and desorption) are used in this article to demonstrate the potential of this model.

There are two major approaches in describing the adsorbent surface heterogeneity. One uses the energy distribution concept and the other considers the heterogeneity in terms of pore-size

Correspondence concerning this article should be addressed to D. Do.

distribution. Although the second approach is more fundamental, the pore-size distribution can be transformed into an energy distribution via some correlation (Dubinin, 1988). Since this article is focused on dynamic problems, only the energy distribution is sufficient to illustrate the role of surface heterogeneity.

Theory

Physical systems and assumptions

Consider a microporous particle of any size exposed to a constant bulk concentration environment. The particle surface is assumed heterogeneous, that is, there exists an interaction energy distribution between adsorbent and adsorbate. The adsorbed species diffuses along the direction of the particle coordinate and along the microparticle direction. The following assumptions are made in the problem formulation.

- The system is isothermal.
- The particle and the microparticle are of either slab, cylinder or sphere.
- The pore diffusivity and film mass-transfer coefficient are constant.
- The surface diffusivity at zero loading is constant.

Local adsorption isotherm and energy distribution

The local adsorption isotherm for a given site with an adsorption energy E is assumed to follow the Langmuir equation, of the following form:

$$C_\mu(E) = C_{\mu s}\frac{b(E)C_p}{1+b(E)C_p} \tag{1}$$

where C_p is the gas phase concentration, $C_{\mu s}$ is the maximum adsorbed phase concentration, $C_\mu(E)$ and $b(E)$ are the adsorbed phase concentration and the affinity for adsorbate for a given site of energy E, respectively, and the affinity is correlated to the interaction energy by the following equation:

$$b(E) = b_0 \exp\left(\frac{E}{RT}\right) \tag{2}$$

Let the energy distribution in the adsorbed phase be $F(E)$, the macroscopically observed isotherm at a given gas phase concentration C_p is:

$$C_{\mu,\text{obs}} = C_{\mu s}\int_0^\infty \frac{b(E)C_p}{1+b(E)C_p}F(E)dE \tag{3}$$

where the energy distribution function satisfies the following equation:

$$\int_0^\infty F(E)dE = 1 \tag{4}$$

Although various energy distribution functions can be used, we will focus ourself on the uniform energy distribution, which has the following form

$$F(E) = \frac{1}{E_{\max}-E_{\min}} \text{ for } E_{\min} < E < E_{\max} \tag{5}$$

and $F(E)=0$ elsewhere. Other distributions can also be dealt with by the theory proposed in this article. Substitution of Eq. 5 into Eq. 3 yields the following Unilan adsorption isotherm (Myers, 1984):

$$C_{\mu,\text{obs}} = C_{\mu s}\left[\frac{1}{2s}\,ln\left(\frac{1+\bar{b}e^{s}C_p}{1+\bar{b}e^{-s}C_p}\right)\right] \tag{6}$$

where

$$\bar{b} = b_0\exp\left(\frac{\bar{E}}{RT}\right);\quad s=\frac{E_{\max}-E_{\min}}{2RT};\quad \bar{E}=\frac{E_{\max}+E_{\min}}{2} \tag{7}$$

The local flux of the adsorbed species

The flux of the adsorbed species at the energy level E is assumed to follow the following equation (Do and Hu, 1992):

$$J_\mu(E) = -\frac{D_\mu(E)}{\left[1-\dfrac{C_\mu(E)}{C_{\mu s}}\right]}\frac{\partial C_\mu(E)}{\partial r} \tag{8}$$

where $D_\mu(E)$ is the surface diffusivity of the energy level E at zero loading, and it is assumed to take the following temperature dependent form:

$$D_\mu = D_{\mu 0}\exp\left(-\frac{aE}{RT}\right) \tag{9}$$

where $D_{\mu 0}$ is the surface diffusivity of the adsorbed species having zero interaction surface energy. The parameter a in Eq. 9 has been observed experimentally to take a value ranging from 0.3 to 0.8 (Kapoor and Yang, 1990; Kapoor et al., 1989).

If the particle size is moderate, one would expect that the diffusion process along the particle coordinate is not the only controlling resistance contributed to the overall mass transfer. The additional resistance is the resistance inside the microparticle, adding to the resistance along the particle coordinate. It is the direction that the adsorbed molecules have to diffuse into its own domain of microparticle (Hu and Do, 1992b). The diffusion path length of this direction is generally much shorter than the diffusion path length of the particle coordinate.

Now we denote the coordinate along the particle being r with a diffusion length of R, and that in the grain being r_μ with a diffusion length of R_μ. The adsorbed phase is considered to have a geometry of slab, cylinder or sphere. The zero coverage surface diffusivity with zero energy, $D_{\mu 0}$, is assumed to be different in the grain coordinate from that in the particle coordinate by a factor of β^2, that is $D_{\mu 0}(r_\mu) = \beta^2 D_{\mu 0}(r)$. We attribute this to the different tortuosity of the adsorbed phase diffusion in different directions. Because activated carbon has been shown to have a micropore distribution, different species with different molecular sizes can access the micropores with different degrees; therefore, this parameter β is not just a function of the medium, but also on the adsorbate as well. Now we can write the fluxes of the adsorbed species at the

energy level E along the corresponding two coordinates as follows:

$$[J_\mu(E)]_r = -\frac{D_\mu(E)}{\left[1-\frac{C_\mu(E)}{C_{\mu s}}\right]}\frac{\partial C_\mu(E)}{\partial r} \tag{10}$$

$$[J_\mu(E)]_{r_\mu} = -\frac{\beta^2 D_\mu(E)}{\left[1-\frac{C_\mu(E)}{C_{\mu s}}\right]}\frac{\partial C_\mu(E)}{\partial r_\mu} \tag{11}$$

with $D_\mu(E)$ following the correlation of Eq. 9.

Mass balance equations

The mass balance equation in the microparticle is

$$\frac{\partial}{\partial t}\int_0^\infty C_\mu(E)F(E)dE = -\frac{1}{r_\mu^{s_\mu}}\frac{\partial}{\partial r_\mu}\left(r_\mu^{s_\mu}\int_0^\infty [J_\mu(E)]_{r_\mu}F(E)dE\right) \tag{12}$$

where s_μ is the geometric factor of the microparticle (=0, 1 and 2 for slab, cylinder and sphere, respectively), and the flux $[J_\mu(E)]r_\mu$ is given in Eq. 11.

In Eq. 12, the parallel-path model (PPM) by Kapoor and Yang (1989) has been adopted to describe the diffusion of adsorbed species. By assuming that the adsorbed phase consists of a series of parallel paths such that each path has a uniform but different energy, and the adsorbed species diffuse in the direction of these parallel paths, the PPM has a comparable accuracy with a two-dimensional effective medium approximation (Kapoor and Yang, 1990) where the diffusion of molecules from one patch of energy to another patch of different energy is allowed.

We note that in Eq. 12, the local concentration of the adsorbed species inside the microparticle, $C_\mu(E)$, is required. There exists an imaginary gas phase concentration, C_{im}, which is in equilibrium with the local observed concentration of the adsorbed species inside the microparticle (Hu and Do, 1992b), that is

$$C_{\mu,\mathrm{obs}}(r_\mu) = \int_0^\infty C_\mu(E)F(E)dE = C_{\mu s}\int_0^\infty \frac{b(E)C_{im}}{1+b(E)C_{im}}F(E)dE \tag{13}$$

The imaginary gas phase concentration can be calculated from the above equation in terms of the local observed adsorbed concentration inside the microparticle, which is obtained from the mass balance equation in the microparticle (Eq. 12). For the uniform energy distribution, we have the Unilan isotherm (Eq. 6) and the imaginary gas phase concentration is

$$C_{im} = \frac{\exp\left(2s\frac{C_{\mu,\mathrm{obs}}(r_\mu)}{C_{\mu s}}\right)-1}{\bar{b}e^{-s}\left[e^{2s}-\exp\left(2s\frac{C_{\mu,\mathrm{obs}}(r_\mu)}{C_{\mu s}}\right)\right]} \tag{14}$$

Therefore, the local adsorbed concentrations inside the microparticle are written in terms of this imaginary gas phase concentration, which the local observed adsorbed concentrations are in equilibrium with.

$$C_\mu(E) = C_{\mu s}\frac{b(E)C_{im}}{1+b(E)C_{im}} \tag{15}$$

The corresponding boundary conditions of Eq. 12 are

$$r_\mu = 0; \quad \frac{\partial C_\mu(E)}{\partial r_\mu} = 0 \tag{16}$$

$$r_\mu = R_\mu; \quad \int_0^\infty C_\mu(E)F(E)dE = \int_0^\infty C_{\mu s}\frac{b(E)C_{p|r}}{1+b(E)C_{p|r}}F(E)dE \tag{17}$$

Equation 17 implies that the adsorbed species at the exterior surface of the microparticle is in local equilibrium with the free species of the macropore.

The total mass balance equation along the particle coordinate is

$$\epsilon_M\frac{\partial C}{\partial t} + (1-\epsilon_M)\frac{\int_0^{R_\mu}\frac{\partial}{\partial t}\left(\int_0^\infty C_\mu(E)F(E)dE\right)r_\mu^{s_\mu}\,dr_\mu}{\int_0^{R_\mu} r_\mu^{s_\mu}\,dr_\mu} = -\epsilon_M\frac{1}{r^s}\frac{\partial}{\partial r}[r^s J_p] - (1-\epsilon_m)\frac{1}{r^s}\frac{\partial}{\partial r}\left[r^s\frac{\int_0^{R_\mu}\left(\int_0^\infty [J_\mu(E)]_r F(E)dE\right)r_\mu^{s_\mu}\,dr_\mu}{\int_0^{R_\mu} r_\mu^{s_\mu}\,dr_\mu}\right] \tag{18}$$

where J_p is the molar flux in the pore phase, ϵ_M is the macropore porosity and s is the particle shape factor, with a value of 1, 1 or 2 being for slab, cylinder or sphere, respectively, and ϵ_M is the macropore porosity. The local adsorbed concentration inside the microparticle is calculated from Eqs. 14 and 15.

The first term in the LHS and RHS of Eq. 18 are self-explainable. The second terms in the LHS and RHS are the average accumulation and the average mass transfer along the particle coordinate contributed by the diffusion of the adsorbed species, respectively.

The boundary conditions of the mass balance equation in the macropore are:

$$r = 0; \quad \frac{\partial C_p}{\partial r} = 0 \tag{19}$$

$$r = R; \quad \epsilon_M J_p + (1-\epsilon_M)\frac{\int_0^{R_\mu}\left(\int_0^\infty [J_\mu(E)]_r F(E)dE\right)r_\mu^{s_\mu}\,dr_\mu}{\int_0^{R_\mu} r_\mu^{s_\mu}\,dr_\mu} = k_m[C_p - C_b] \tag{20}$$

The initial conditions of the model equations are:

$$t=0;\quad C_p=C_{pi};\quad C_\mu(E)=C_{\mu s}\frac{b(E)C_{pi}}{1+b(E)C_{pi}} \tag{21}$$

The above set of model equations (Eqs. 12 to 21) represent a very general mathematical formulation of adsorption and desorption in a heterogeneous microporous particle of any size, in which the adsorbed phase is heterogeneous in structure, characterized by an energy distribution, unique for a given adsorbate-adsorbent pair.

If the particle is large enough or the microparticle diffusion path R_μ/β is very small, that is,

$$\frac{R_\mu^2}{\beta^2 D_\mu(E_{\max})}<<\frac{R^2}{D_\mu(E_{\min})} \tag{22}$$

this model is reduced to the model proposed recently by Do and Hu for large particles (1992).

However, when

$$\frac{R_\mu^2}{\beta^2 D_\mu(E_{\min})}>>\frac{R^2}{D_\mu(E_{\max})} \tag{23}$$

one would expect the diffusion into the grain is dominating the kinetics of adsorption. For such cases, the mass balance equations then become

$$\frac{\partial}{\partial t}\int_0^\infty C_\mu(E)F(E)dE=-\frac{1}{r_\mu^{s_\mu}}\frac{\partial}{\partial r_\mu}\left(r_\mu^{s_\mu}\int_0^\infty J_\mu(E)F(E)dE\right) \tag{24}$$

$$r_\mu=0;\quad \frac{\partial C_\mu(E)}{\partial r_\mu}=0 \tag{25}$$

$r_\mu=R_\mu$;

$$\int_0^\infty C_\mu(E)F(E)dE=\int_0^\infty C_{\mu s}\frac{b(E)C_{p|R}}{1+b(E)C_{p|R}}F(E)dE \tag{26}$$

which are the model equations to describe mass transport into the adsorbed phase along the microparticle coordinate only.

When the adsorbed phase is homogeneous (that is, there is only one energy site), this model is reduced to the micropore, surface and micropore diffusion (MSMD) model recently proposed by Hu and Do (1992b). The model is even further reduced to the Constant surface diffusivity Macropore, Surface and Micropore Diffusion (CMSMD) model by Do and co-workers (Gray and Do, 1990; Mayfield and Do, 1991) if the surface diffusivities are assumed concentration independent. For convenience, we will call the current theory as Heterogeneous Macropore, Surface and Micropore Diffusion (HMSMD) model.

Nondimensional Mass Balance Equations

We have presented in the last section a new mathematical model to describe adsorption and desorption dynamics into heterogeneous microporous particles of any size. To facilitate with the numerical computation, the model equations are cast into nondimensional form by using the nondimensional variables and parameters defined in Table 1.

Table 1. Definitions of Nondimensional Variables and Parameters

$$e=\frac{E}{RT};\quad f(e)=F(E)RT;\quad \bar{e}=\int_0^\infty ef(e)de$$

$$\lambda(e)=b_0\exp(e)C_o;\quad H(e)=\exp[a(\bar{e}-e)]$$

$$Y=\frac{C_p}{C_o};\quad Y_b=\frac{C_b}{C_o};\quad Y_{im}=\frac{C_{im}}{C_0}$$

$$Y_\mu(e)=\frac{C_\mu(E)}{C_{\mu o}};\quad C_{\mu o}=C_{\mu s}\int_0^\infty\frac{\lambda(E)}{1+\lambda(E)}f(e)de$$

$$x=\frac{r}{R};\quad x_\mu=\frac{r_\mu}{R_\mu}$$

$$\tau=\frac{(\epsilon_M D_p C_0+(1-\epsilon_M)D_{\mu 0}e^{-a\bar{e}}C_{\mu 0})t}{R^2[\epsilon_M C_0+(1-\epsilon_M)C_{\mu 0}]}$$

$$\sigma=\frac{\epsilon_M C_0}{\epsilon_M C_0+(1-\epsilon_M)C_{\mu 0}};\quad \sigma_\mu=1-\sigma$$

$$\eta=\frac{\epsilon_M D_p C_0}{\epsilon_M D_p C_0+(1-\epsilon_M)D_{\mu 0}e^{-a\bar{e}}C_{\mu 0}}$$

$$\delta=\frac{(1-\epsilon_M)D_{\mu 0}e^{-a\bar{e}}C_{\mu 0}}{\epsilon_M D_p C_0+(1-\epsilon_M)D_{\mu 0}e^{-a\bar{e}}C_{\mu 0}}$$

$$\gamma=\delta\left(\frac{\beta R}{R_\mu}\right)^2$$

$$Bi=\frac{k_m R C_0}{\epsilon_M D_p C_0+(1-\epsilon_M)D_{\mu 0}e^{-a\bar{e}}C_{\mu 0}}$$

C_o is the reference gas phase concentration.

In nondimensional form, the mass balance equations (Eqs. 12, 16 to 20) become

$$\sigma_\mu\frac{\partial}{\partial\tau}\int_0^\infty f(e)Y_\mu(e)de=\gamma\frac{1}{x_\mu^{s_\mu}}\frac{\partial}{\partial x_\mu}\times\left(x_\mu^{s_\mu}\int_0^\infty\frac{H(e)}{\left[1-\left(\frac{C_{\mu 0}}{C_{\mu s}}\right)Y_\mu(e)\right]}\frac{\partial Y_\mu(e)}{\partial x_\mu}f(e)de\right) \tag{27}$$

$$x_\mu=0;\quad \frac{\partial Y_\mu(e)}{\partial x_\mu}=0 \tag{28}$$

$$x_\mu=1;\quad \int_0^\infty Y_\mu(e)f(e)de=\frac{C_{\mu s}}{C_{\mu 0}}\int_0^\infty\left[\frac{\lambda(e)Y}{1+\lambda(e)Y}\right]_x f(e)de \tag{29}$$

$$\sigma \frac{\partial Y}{\partial \tau} + \sigma_\mu \frac{\int_0^1 \left(\frac{\partial}{\partial \tau} \int_0^\infty Y_\mu(e) f(e) de \right) x_\mu^{s_\mu} dx_\mu}{\int_0^1 x_\mu^{s_\mu} dx_\mu}$$

$$= \eta \frac{1}{\partial x^s} \frac{\partial}{\partial x} \left(x^s \frac{\partial Y}{\partial x} \right) + \delta \frac{1}{x^s} \frac{\partial}{\partial x}$$

$$\left\{ \times x^s \frac{\int_0^1 \left(\int_0^\infty \frac{H(e)}{\left[1 - \left(\frac{C_{\mu 0}}{C_{\mu s}} \right) Y_\mu(e) \right]} \frac{\partial Y_\mu(e)}{\partial x} f(e) de \right) x_\mu^{s_\mu} dx_\mu}{\int_0^1 x_\mu^{s_\mu} dx_\mu} \right\} \tag{30}$$

$$x = 0; \quad \frac{\partial Y}{\partial x} = 0 \tag{31}$$

$$x = 1; \ \eta \frac{\partial Y}{\partial x}$$

$$+ \delta \frac{\int_0^1 \left\{ \int_0^\infty \frac{H(e)}{\left[1 - \left(\frac{C_{\mu 0}}{C_{\mu s}} \right) Y_\mu(e) \right]} \frac{\partial Y_\mu(e)}{\partial x} f(e) de \right\} x_\mu^{s_\mu} dx_\mu}{\int_0^1 x_\mu^{s_\mu} dx_\mu}$$

$$= Bi(Y_b - Y) \tag{32}$$

The parameter γ signifies the ratio of the diffusion time scale in the particle coordinate to that in the microparticle. When it is very large, that is, the resistance in the microparticle is negligible compared to that in the macropore, the model is reduced to the macropore and surface diffusion controlling mechanism (Do and Hu, 1992). When γ is very small, the micropore resistance will dominate the mass-transfer process inside the particle.

Solution method

A RADAU quadrature (Villadsen and Michelsen, 1978) is used to evaluate the integrals involving the energy distribution:

$$\int_0^\infty J_\mu(E) F(E) dE = \int_0^1 J_\mu(x_e) g(x_e) dx_e$$

$$= \sum_{ig=1}^{NT} J_\mu[x_e(ig)] g[x_e(ig)] we(ig) \tag{33}$$

where x_e is a variable used to normalize the integral range and $we(ig)$ is the quadrature weight at each node point $x_e(ig)$. In particular, for a uniform energy distribution, we have

$$F(E) = \frac{1}{E_{\max} - E_{\min}} \text{ for } E_{\min} < E < E_{\max} \tag{34}$$

and $F(E) = 0$ elsewhere. Hence,

$$x_e = \frac{E - E_{\min}}{E_{\max} - E_{\min}}; \quad g(x_e) = 1 \tag{35}$$

and

$$E = E_{\min} + x_e(E_{\max} - E_{\min}) \tag{36}$$

The average accumulation of the adsorbed species within the microparticle

$$\frac{\int_0^1 \left(\frac{\partial}{\partial \tau} \int_0^\infty Y_\mu(e) f(e) de \right) x_\mu^{s_\mu} dx_\mu}{\int_0^1 x_\mu^{s_\mu} dx_\mu} \tag{37}$$

is also integrated by using the RADAU quadrature. The average diffusion flux of the adsorbed species along the particle coordinate is solved by a similar technique.

The nondimensional mass balance equations (Eqs. 27-32) are then numerically solved by using a combination of the orthogonal collocation technique of Villadsen and Michelsen (1978) to transform the coupled partial differential equations to a larger set of coupled ordinary differential equations and the differential-algebraic equation solver (Petzold, 1982). The simulations were carried out on a personal computer of 33 MHz 80386/80387, and the time of execution ranges from 3 to 10 minutes, depending on the number of collocation points and the number of quadrature points used.

Experiments

Dynamics measurement

The adsorbent used in this study is Activated carbon Type 976, supplied by Ajax Chemical Co., Australia as 1/16 in. diameter cylindrical extrudates. The structural properties of Ajax carbon were characterized by Gray and Do (1989) and relisted in Table 2 for conveniences. The preparations of slab and cylinder particles, the experimental apparatus (Differential Adsorption Bed) and techniques are similar to those in Do et al. (1991). The isothermal condition is justified by the high flow rate of the adsorbate and from a thermocouple inserted inside the adsorber. It is also recognized that the temperature gradient within the particle during adsorption is usually small and can be ignored since the effective thermal conductivities for the commercial sorbent pellets are relatively high (Yang, 1987). The experimental procedures are briefly stated as follows.

- The adsorption bed was initially heated up to a high temperature (150°C) under vacuum overnight and then degassed by purging the heated bed with a small flow of pure nitrogen for 15 minutes.
- The bed was brought to the adsorption temperature using a water bath and the adsorbate was flushed to the bed at a flow rate of 500 cm^3/min for a predetermined adsorption time before the adsorber was isolated.
- The sample was desorbed to a pre-evacuated bomb by heating up the adsorption bed to the desorption temperature (100°C for ethane, 150°C for propane) and then further desorbed by slowly flushing pure nitrogen (around 10 cm^3/min) through the adsorber for 15 minutes.
- The pressure and temperature of the bomb were measured

Table 2. Physical Properties of Ajax Activated Carbon

Particle Bulk Density	660 kg/m^3
Total Porosity	0.71
Macropore Porosity ($>5\times10^{-9}$m)	0.31 m^3 macropore/m^3 particle
Micropore Porosity ($<5\times10^{-9}$m)	0.40 m^3 macropore/m^3 particle
Average Macropore Diameter	8×10^{-7}m
Nitrogen Surface Area	1.2×10^6 m^2/kg

and recorded and then the adsorbate (ethane or propane) concentration in the bomb was analyzed by gas chromatography. The adsorbed amount was calculated by removing the contribution of the adsorbate trapped in the voids of the adsorber at isolation from the total amount in the bomb.

- By repeating the second through fourth steps for different exposure times an uptake curve can be obtained for the specified experimental conditions.
- Desorption experiments which were not done by Do et al. (1991): First, the adsorbate stream was passed through the adsorber sufficiently long enough for the equilibrium to occur. Then pure nitrogen was flushed through the adsorber for a predetermined desorption time. And the same procedure used for kinetic measurements for adsorption was adopted to desorb the remaining adsorbate in the particle.

Equilibrium isothermal measurement.

The adsorption equilibrium data of ethane and propane in Ajax activated carbon were collected via a high accuracy volumetric adsorption isotherm measurement rig which has two separate chambers. One has a supply bomb and the other contains an adsorption cell. Each chamber has a separate MKS transducer to record the pressure. The operation procedures are briefly summarized in follows.

- The whole system is first evacuated to vacuum using an Alcatel molecular drag pump and the activated carbon particles in the adsorption cell are heated up to 300°C and kept at this temperature and under vacuum for overnight to degas any possible adsorbed species.
- Pure gas (ethane or propane) is then dosed into the supply bomb and the pressure and temperature are recorded when constant readings are reached.
- A small amount of pure gas is dosed from the supply bomb into the adsorption cell which is kept isothermal by using a water bath. After the pressure in the adsorption cell becomes constant (typically about two hours), the pressures and temperatures in both supply bomb and cell are recorded.
- The amount adsorbed which is in equilibrium with the pressure in the gas phase of the cell is calculated from the amount supplied from the supply bomb via the ideal P-V-T relationship.
- Repeat the fourth and fifth steps to get the equilibrium isotherm data at higher pressures until a full isotherm curve is obtained.

Results and Discussions

Adsorption equilibrium isotherms

The adsorption equilibria of ethane and propane on Ajax activated carbon are measured at three temperatures, 10°, 30° and 60°C. Figure 1a shows the isotherm data of ethane/carbon. The isotherm data of propane/carbon are plotted in Figure 1b. All data sets are fitted to the Langmuir and the Langmuir-Uniform distribution equations. When fitting the data to the latter isotherms, the parameters E_{min}, E_{max} and b_0 were set to be temperature independent but species dependent, while the saturation parameter, $C_{\mu s}$, was set to the same for ethane and propane but temperature dependent. The reason for this is that the identical values of $C_{\mu s}$ for different species are required for the local extended Langmuir isotherm to be thermodynamically consistent in the future studies of multicomponent sorption dynamics. All the experimental data at three temperatures for ethane and propane were fitted to the Langmuir-Uniform distribution isotherm simultaneously by nonlinear regression. The extracted parameters for both isotherm models are tabulated in Tables 3 and 4. A little surprising is that the saturation capacity ($C_{\mu s}$) of the Unilan isotherm at 60°C is a bit larger than that at 10 or 30°C. This could be due to the fact that no data at higher pressure (>130 kPa) are available, which are needed to accurately determine the maximum adsorption capacity. A similar temperature trend of the saturation capacity is also seen in Kapoor and Yang (1989) and Moon and Tien (1988). The solid lines in Figure 1 are the fitted isotherms of Langmuir-Uniform distribution and the dashed lines are Langmuir isotherms. The Langmuir-Uniform distri-

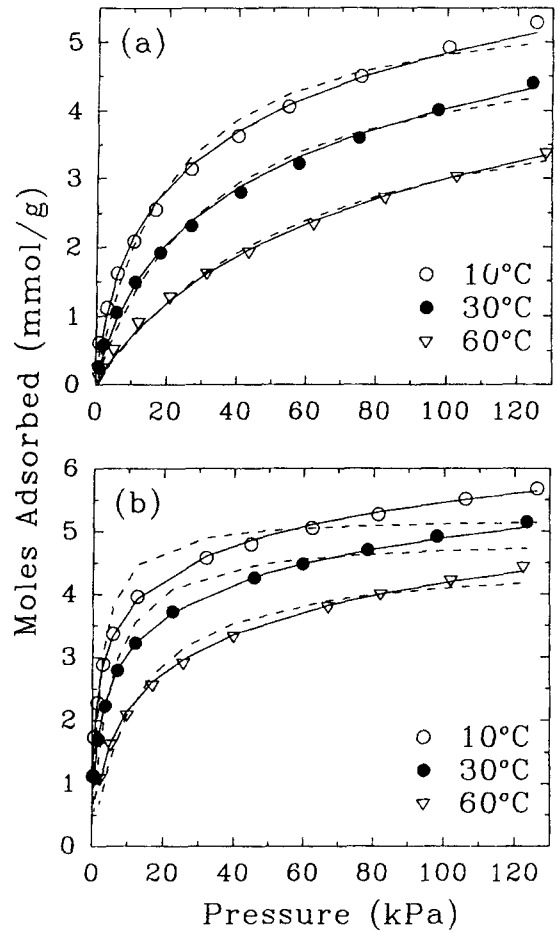

Figure 1. Effect of energy distribution on the adsorption equilibrium isotherms of ethane and propane on Ajax activated carbon.

(a) Ethane/carbon; (b) Propane/carbon. —— Langmuir-Uniform distribution isotherm; — — — Langmuir isotherm.

Table 3. Isotherm Parameters for Ethane/Ajax Activated Carbon

Temperature (°C)	Langmuir-Uniform Distribution Isotherm (Unilan) $C_{\mu s}$ (kmol/m³)	b (kPa⁻¹)	s	Langmuir Isotherm $C_{\mu s}$ (kmol/m³)	b (kPa⁻¹)
10°	13.0	2.20×10^{-3}	5.20	5.49	0.0516
30°	13.0	1.31×10^{-3}	4.86	5.00	0.0320
60°	13.4	6.77×10^{-4}	4.42	4.58	0.0167
b_0(kPa⁻¹)		8.47×10^{-7}			
E_{min}(kJoule/mol)		6.26			
E_{max}(kJoule/mol)		30.75			

bution model fits the experimental data very well even when the above mentioned restrictions are applied, and the Langmuir model also fits the ethane/carbon data well but fails to be in good agreement with the propane/carbon data.

Sorption kinetics

The theory we presented in the theory section is now validated using the experimental dynamic results of the adsorption and desorption of ethane and propane onto Ajax activated carbon.

Figure 2 shows the fit between our dynamic theory and the experimental data sets of three different external bulk ethane concentrations (20%, 10%, and 5%) for three particle sizes (4.4 and 2.6 mm full length slabs and 1/16 in. diameter cylinder) at 30°C and 1 atm. The ratio of the surface diffusion activation energy to the heat of adsorption, a, is taken to be 0.5, and the microparticle is assumed to have a spherical geometry ($s_\mu = 2$), although other geometries can also be assumed and a different value of R_μ/β obtained. Thus, the fitting parameters in Figure 2 are pore diffusivity D_p, zero coverage surface diffusivity at zero energy level $D_{\mu 0}$ and R_μ/β, which is the diffusion path length in the grain direction divided by the square root of the ratio of zero coverage surface diffusivity at zero energy level in microparticle direction to that in the particle direction. We call this parameter, R_μ/β, the effective diffusion length in the microparticle direction. The diffusion path length in the grain direction, R_μ, is independent of the adsorbate but a function of the adsorbent structure only. While β is supposed to be dependent on the solid medium and the access degree of the adsorbate to the micropores of the adsorbent, both R_μ and β are assumed to be temperature and concentration independent. The effective diffusion length in the grain direction, R_μ/β, is found to be 6.95×10^{-4} m, the zero coverage surface diffusivity at zero energy level $D_{\mu 0}$ is 1.78×10^{-7} m²/s and the pore diffusivity at 30°C is 4.48×10^{-6} m²/s for ethane/Ajax activated carbon. The pore diffusivity gives a macropore tortuosity of 3.0 (using the calculated combined Knudsen and molecular diffusivity of 1.34×10^{-5} m²/sec) which is at the lower end of the range expected for carbons (Yang, 1987). This macropore tortuosity is smaller than the value of 8 reported by Do and co-workers (Gray and Do, 1990; Mayfield and Do, 1991). The reason for this may be that in the attempts to determine the tortuosity, they used the macropore diffusion control model to analyze the experimental data (Mayfield, 1990). This way there might be some contribution of the micropore resistance in the calculation of the macropore tortuosity. A tortuosity of three was previously obtained when a macropore and micropore diffusion control model was used (Gray, 1991).

The macropore tortuosity of three will then be used in all other dynamic analyses. That is, the pore diffusivities are calculated from the Knudsen and molecular diffusivities (Reid et al., 1987) and the tortuosity of three used. Therefore, the pore diffusivity is not a fitting parameter any more, but calculated *a priori*.

It is expected that the micropore tortuosity factor is much higher than the macropore one. Hence, the parameter β will be a small number so that the real microparticle size R_μ is much smaller than the effective diffusion length in the microparticle direction.

We note that the model fittings with the data for cylinder particles are not as good as that for slab particles. This might be explained by the nonisothermal effect, because the adsorption rate in 1/16 in. cylinders is more rapid than that in large slab particles. A small temperature rise (<4°C) is experimentally observed during the initial stage of adsorption (<50 seconds).

The fittings of the MSMD (dashed lines) and CMSMD (dashed-dotted lines) are also plotted in Figure 2. The equilibrium equations used is Unilan isotherm, which is identical to the Langmuir-Uniform distribution, for both MSMD and

Table 4. Isotherm Parameters for Propane/Ajax Activated Carbon

Temperature (°C)	Langmuir-Uniform Distribution Isotherm (Unilan) $C_{\mu s}$ (kmol/m³)	$\bar{b}$ (kPa⁻¹)	s	Langmuir Isotherm $C_{\mu s}$ (kmol/m³)	b (kPa⁻¹)
10°	13.0	1.70×10^{-3}	9.08	5.00	0.470
30°	13.0	9.34×10^{-4}	8.48	4.69	0.217
60°	13.4	4.35×10^{-4}	7.72	4.36	0.0863
b_0(kPa⁻¹)		1.93×10^{-7}			
E_{min}(kJoule/mol)		0.0			
E_{max}(kJoule/mol)		42.75			

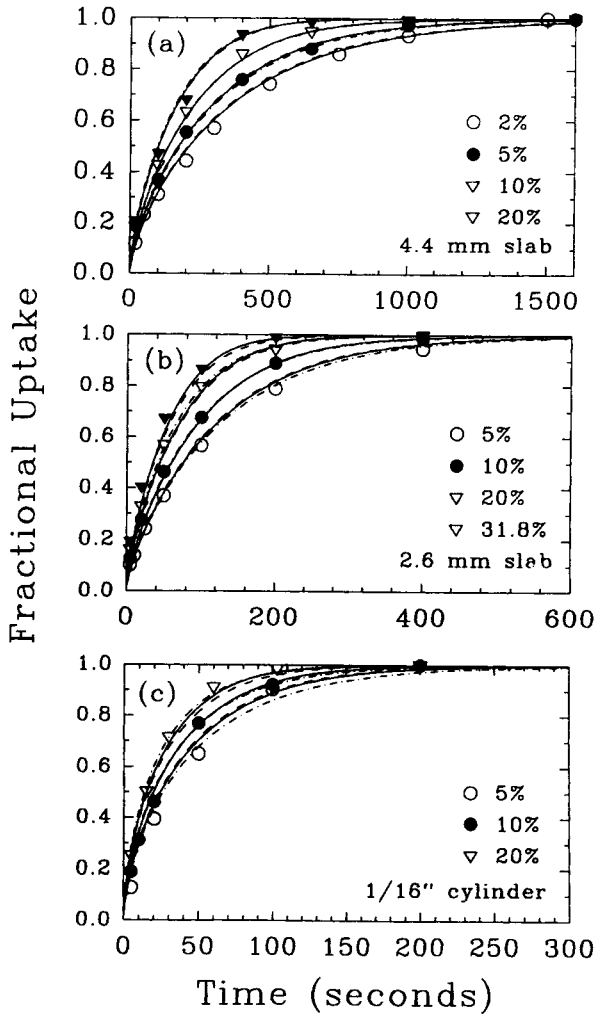

Figure 2. Adsorption dynamics of ethane/Ajax activated carbon at 30°C, 1 atm.

—— HMSMD model; - - - - - MSMD model; - · - · - · - CMSMD model.

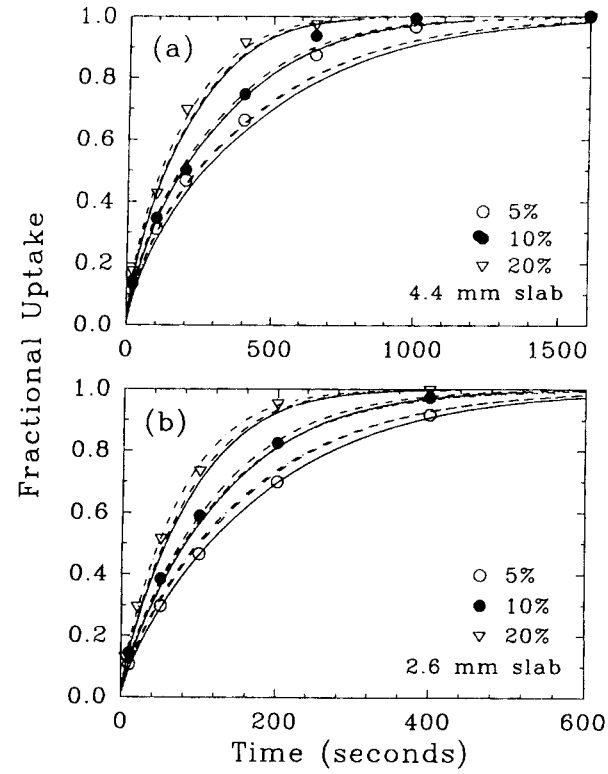

Figure 3. Adsorption dynamics of ethane/Ajax activated carbon at 10°C, 1 atm.

—— HMSMD model; - - - - - MSMD model; - · - · - · - CMSMD model.

CMSMD models for better comparisons of the dynamic factor. The extracted effective diffusion length in the microparticle direction, R_μ/β, from the MSMD model is also used in the CMSMD model for comparison reasons and due to the fact that there are more parameters in the CMSMD model. Although all three models can fit the data well, the CMSMD model has to use different surface diffusivities for different bulk concentrations (Table 5), which is apparently in conflict with its assumption of "constant surface diffusivity." It is even worse that some of the surface diffusivities do not show

Table 5. Dynamic Parameters of Ethane/Ajax Activated Carbon

	Temperature (°C)	D_p (10^{-6}m^2/s)	D_μ (10^{-10}m^2/s)	R_μ/β(10^{-4}m)
CMSMD Model	10°	4.03	11.1 (5%) 10.1 (10%) 19.7 (20%)	6.91
	30°	4.48	8.94 (5%) 11.9 (10%) 16.2 (20%)	
	60°	5.23	8.12 (5%) 1.55 (10%) 2.56 (20%)	
MSMD Model	10°	4.03	7.58	
	30°	4.48	8.72	
	60°	5.23	13.4	
HMSMD Model	10°	4.03		
	30°	4.48	1,780*	6.95
	60°	5.23		

* Value reported is $D_{\mu 0}$

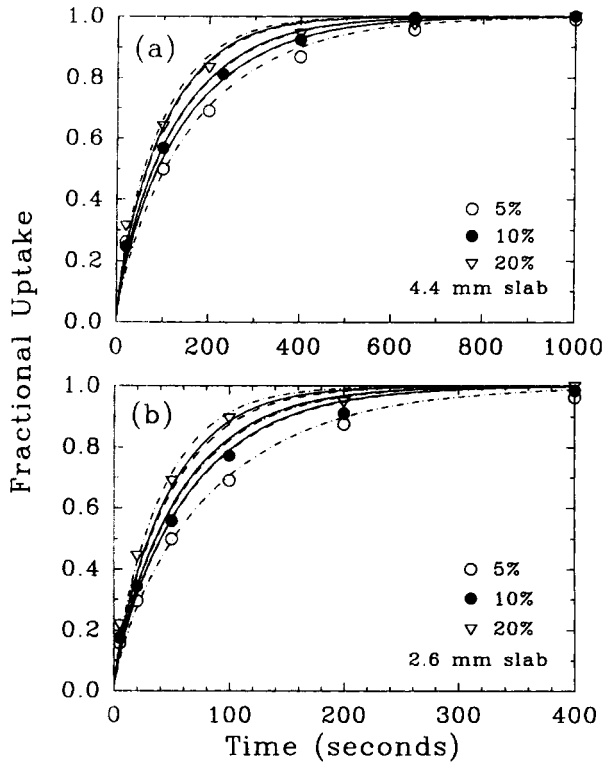

Figure 4. Adsorption dynamics of ethane/Ajax activated carbon at 60°C, 1 atm.

—— HMSMD model; - - - - - MSMD model; - · - · - · - CMSMD model.

the correct dependency trends of temperature and concentration. For example, the surface diffusivity at 5%, 10°C is higher than that at 5%, 30°C or 10%, 10°C (Table 5), which should not be physically expected. In the studies of Gray (1991) and Mayfield (1990), they also reported the different surface diffusivities for different external bulk concentrations. Both MSMD and HMSMD models are in good agreement with the experimental data of different bulk concentrations and particle sizes with their unique zero coverage surface diffusivities. The advantage of the HMSMD model is that only one zero coverage surface diffusivity at zero energy level is required and hence it can predict the uptake rates at different temperatures (10 and 60°C) because no extra fitting parameters are needed, while the MSMD model requires different values of the parameter $D_{\mu 0}$. Therefore, the HMSMD model reflects the true diffusion mechanism of adsorbed species. The model fittings and experimental data of ethane adsorption on Ajax slab activated carbon of 4.4 and 2.6 mm length at 10 and 60°C are shown in Figures 3 and 4. Similar conclusions to those of ethane/carbon adsorption at 30°C are observed. The fittings are good in all cases except for ethane adsorption on 2.6 mm slab carbon at 60°C where some deviations exist.

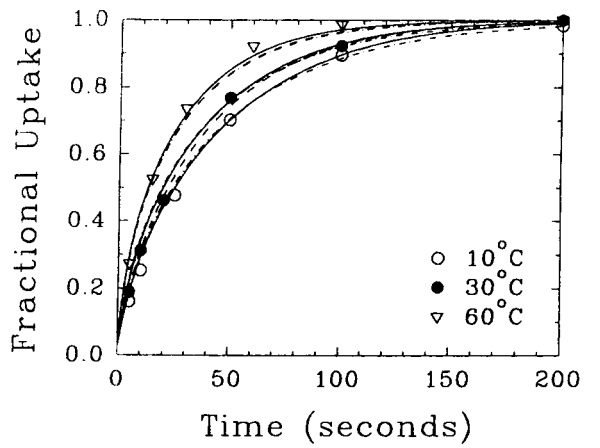

Figure 5. Effect of temperature on adsorption dynamics of 10% ethane on 1/16″ cylindrical Ajax activated carbon at 1 atm.

—— HMSMD model; - - - - - MSMD model; - · - · - · - CMSMD model.

The effect of temperature on the adsorption rate of 10% ethane on 1/16 in. cylinder Ajax carbon is plotted in Figure 5. The uptake rate increases as temperature increases, which is physically expected because the surface diffusivity increases with temperature. Again the model fittings are in good agreement with the experimental data. A summary of the errors and number of adjustable parameters for Ethane/Carbon adsorption kinetics at 10, 30 and 60°C and concentrations of 5%, 10% and 20% of three different models is listed in Table 6.

All three models are further tested by applying them to predict the ethane/carbon desorption dynamics using the parameters extracted from the adsorption kinetics. Here the disadvantage of the CMSMD model is clearly seen. Although it can fit the data reasonably well by adjusting the surface diffusivity for different external bulk concentrations, it overpredicts the desorption kinetics data. This model also fails to predict the less sensitivity of the concentration dependency of desorption rate (Figure 6b) than that of adsorption (Figure 2b) which is well described by the experimental data and the MSMD and HMSMD models. The predictions of MSMD and HMSMD models are in reasonable good agreement with the experimental data and are superimposed to each other because the effect of energy distribution on the ethane/carbon isotherm is not significant (Figure 1a). The deviations for cylinder particles may be due to the temperature drops (<4°C) in the initial stage of desorption.

Table 6. Errors and Number of Adjustable Parameters for Ethane/Carbon Adsorption Kinetics at 10, 30 and 60°C and Concentrations of 5, 10 and 20%

Model	Temperature (°C)	Error*	Number of Adjustable Parameters
HMSMD	10°	0.045	0
	30°	0.045	2
	60°	0.075	0
MSMD	10°	0.038	1
	30°	0.047	2
	60°	0.075	1
CMSMD	10°	0.026	3
	30°	0.036	3
	60°	0.047	3

*Error reported is the summation of $[F_{up}(\text{model}) - F_{up}(\text{data})]^2$ of all three concentrations.

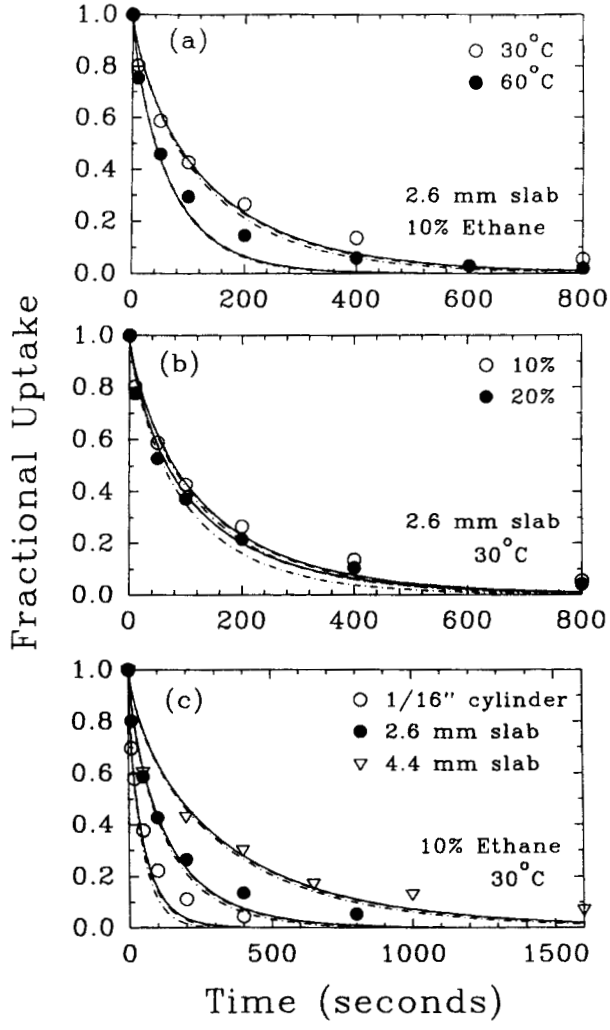

Figure 6. Desorption dynamics of ethane/Ajax activated carbon at 1 atm.

—— HMSMD model; - - - - MSMD model; - · - · - · CMSMD model.

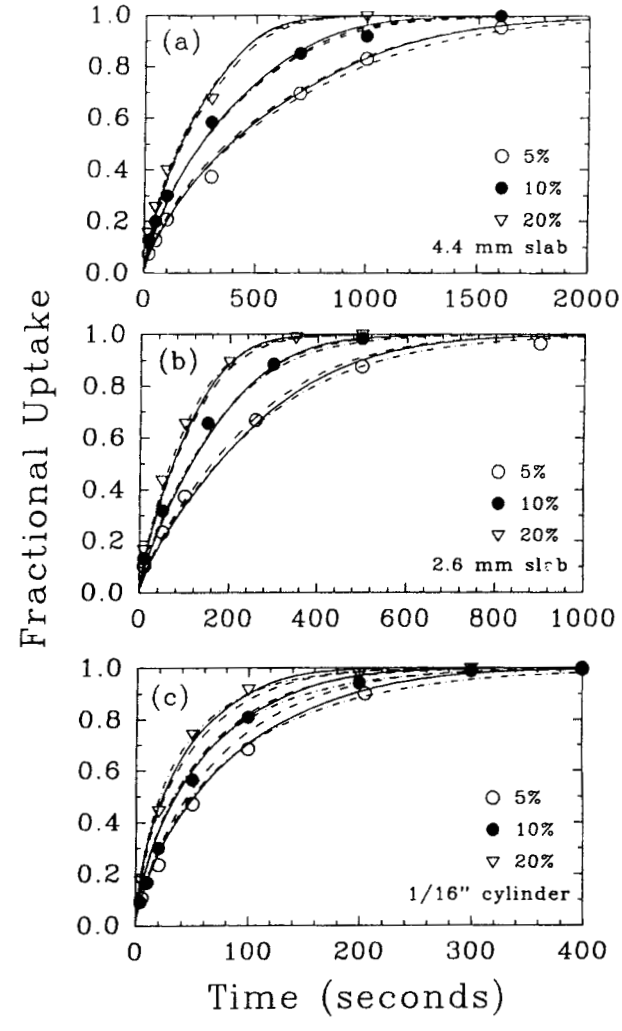

Figure 7. Adsorption dynamics of propane/Ajax activated carbon at 30°C, 1 atm.

—— HMSMD model; - - - - MSMD model; - · - · - · CMSMD model.

Table 7. Dynamic Parameters of Propane/Ajax Activated Carbon

	Temperature (°C)	D_p (10^{-6}m^2/s)	D_μ (10^{-10}m^2/s)	R_μ/β(10^{-4}m)
CMSMD Model	10°	3.20	12.0 (5%) 13.8 (10%) 21.3 (20%)	9.7
	30°	3.47	9.63 (5%) 13.0 (10%) 19.4 (20%)	
	60°	4.16	14.2 (5%) 17.0 (10%) 25.2 (20%)	
MSMD Model	10°	3.20	4.37	
	30°	3.47	5.06	
	60°	4.16	9.47	
HMSMD Model	10°	3.20		
	30°	3.47		
	60°	4.16	7,460*	10.7

*Value reported is $D_{\mu 0}$

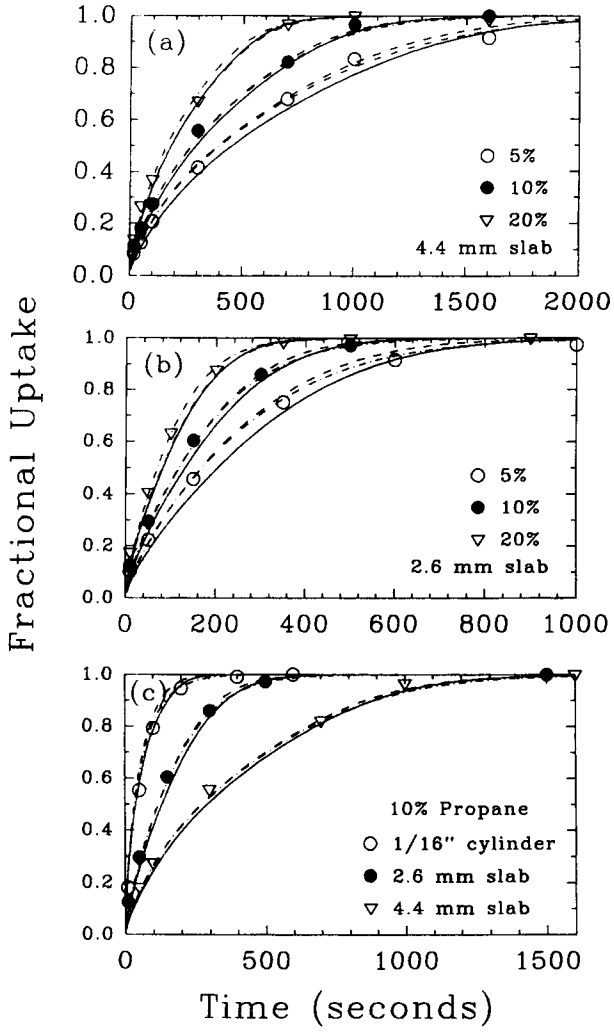

Figure 8. Adsorption dynamics of propane/Ajax activated carbon at 10°C, 1 atm.

—— HMSMD model; - - - - MSMD model; - · - · - CMSMD model.

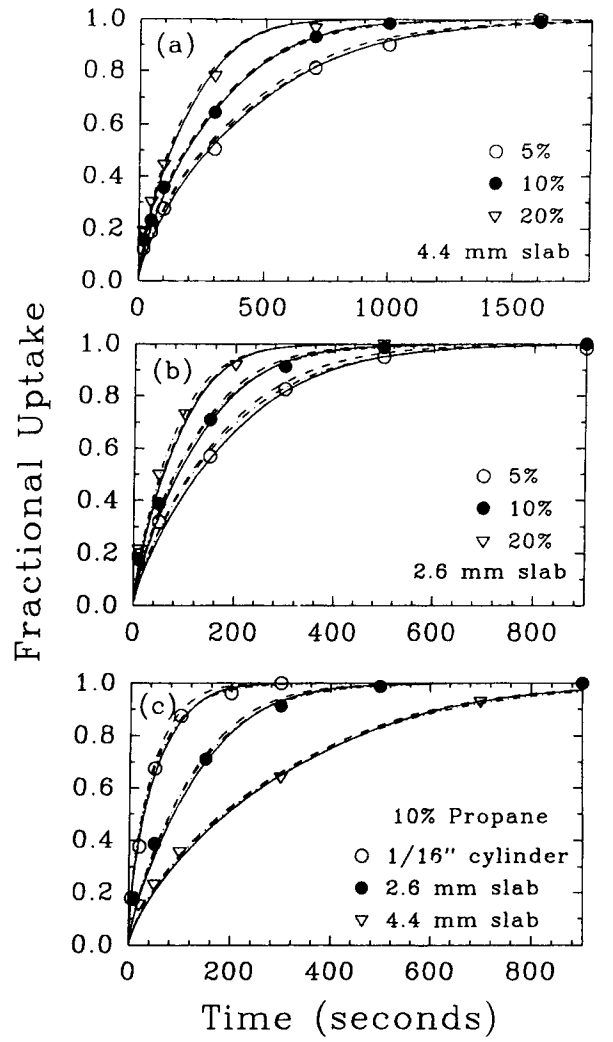

Figure 9. Adsorption dynamics of propane/Ajax activated carbon at 60°C, 1 atm.

—— HMSMD model; - - - - MSMD model; - · - · - CMSMD model.

The extensive adsorption dynamics experimental data of propane on Ajax activated under various conditions, three bulk concentrations (5%, 10% and 20%), three particle sizes (2.6 and 4.4 mm slabs and 1/16 in. cylinder) and three temperatures (10, 30 and 60°C) are used to further validate the proposed theory. The data together with the model fittings are shown in Figures 7 to 9. Since the pore diffusivities are calculated *a priori* from the Knudsen and molecular diffusivities and the macropore tortuosity of three, the fitting parameters are now the zero coverage surface diffusivity at zero energy level and the effective diffusion length in the microparticle direction, R_μ/β, which were found to be 7.46×10^{-7} m^2/s and 10.7×10^{-4} m for propane/carbon adsorption, respectively. All the extracted parameters at different temperatures together with those of the CMSMD and MSMD models are tabulated in Table 7. All three models can fit the data well in all cases, but again the CMSMD requires to use different surface diffusivities for different bulk concentrations and some incorrect temperature dependency trend of the surface diffusivity occurs at the bulk concentration of 5%. The zero coverage surface diffusivity at zero energy level of HMSMD model can be used in all three temperatures. The errors and number of adjustable parameters for Propane/Carbon adsorption kinetics at 10, 30 and 60°C and concentrations of 5%, 10% and 20% of three different models is tabulated in Table 8.

The desorption kinetics of propane/carbon at different temperatures (30 and 60°C), different bulk concentrations (10% and 20%) and different particle sizes (4.4 and 2.6 mm slabs and 1/16 in. cylinder) are used to validate the model. As shown in Figure 10, the predictions of CMSMD model are even worse since the Langmuir equation is in poor agreement with the propane/carbon isotherm, that is, the energy distribution is more significant. The fractional uptake desorption curves are again experimentally found to be not as sensitive to the bulk concentration as the adsorption curves (Figures 10b and 7b). This phenomenon can be well expressed by both MSMD and HMSMD models which are in good agreement with the experimental data. Since the energy distribution is important in the propane isotherm, the predictions of desorption curves of

Table 8. Errors and Number of Adjustable Parameters for Propane/Carbon Adsorption Kinetics at 10°, 30° and 60°C and Concentrations of 5, 10 and 20%

Model	Temperature (°C)	Error*	Number of Adjustable Parameters
HMSMD	10°	0.048	0
	30°	0.054	2
	60°	0.054	0
MSMD	10°	0.038	1
	30°	0.070	2
	60°	0.048	1
CMSMD	10°	0.023	3
	30°	0.055	3
	60°	0.037	3

*Error reported is the summation of $[F_{up}(\text{model}) - F_{up}(\text{data})]^2$ of all three concentrations.

propane from HMSMD are better than those from MSMD model.

Conclusions

We have presented in this article a new model of sorption dynamics for any sized heterogeneous microporous particles. This model takes into account the nature of the energy distribution in both isotherm and dynamics. The diffusion of the adsorbed species occurs in both directions of the particle and microparticle coordinates. The theory was tested with the adsorption and desorption dynamics of ethane and propane on Ajax activated carbon. In all cases tested the theory has shown a great promise as a mathematical tool for studying the dynamics of sorption. The CMSMD model is found to be not a suitable model because it fails to consider the concentration dependency of the surface diffusivity and cannot predict the desorption behaviors. When the energy distribution is not important in the isotherm, the MSMD model can describe the sorption dynamics as good as HMSMD model and is recommended due to its simpler expression. The effect of energy distribution on the prediction of desorption kinetics is significant only when it is also important in the isotherm equilibrium expression. The HMSMD model, however, has another advantage that it has less parameters to be extracted since the zero coverage surface diffusivity at zero energy level is independent of temperature. Therefore, the HMSMD model better describes the intrinsic diffusion mechanism of adsorbed species in activated carbon.

Acknowledgment

This project was funded by the Australian Research Council. Support from the Research Excellence Grants Scheme from the University of Queensland is also gratefully acknowledged.

Notation

a = ratio of the surface activation energy to the heat of adsorption
b = isotherm parameter (m^3/kmol)
b_0 = isotherm parameter (m^3/kmol)
Bi = Biot number defined in Table 1

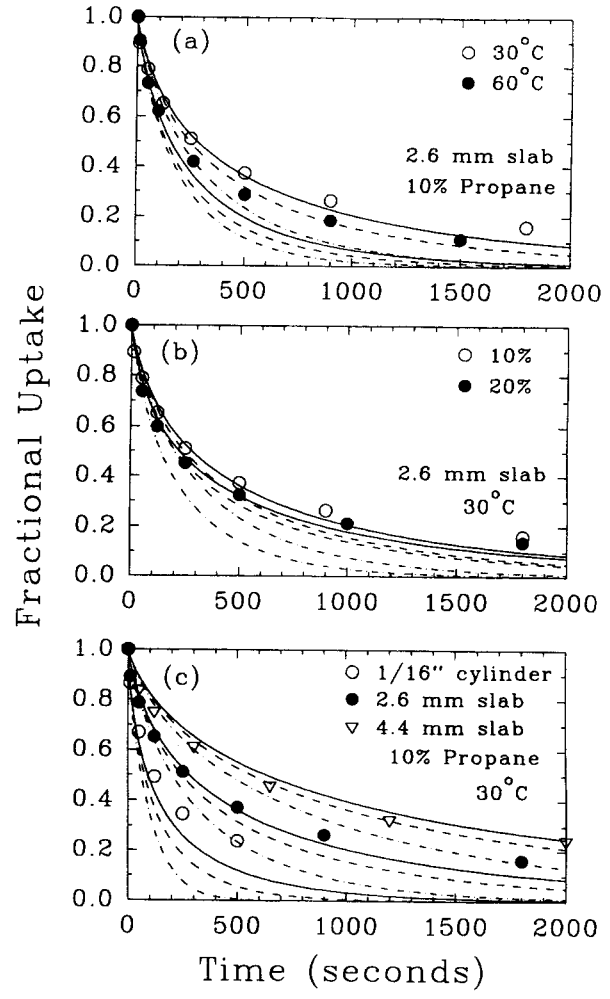

Figure 10. Desorption dynamics of propane/Ajax activated carbon at 1 atm.

—— HMSMD model; - - - - - MSMD model; - - - - - - - CMSMD model.

C_p = adsorbate concentration in the macropore (kmol/m^3)
C_b = adsorbate concentration in the bulk (mol/m^3)
C_i = initial adsorbate concentration in the macropore (kmol/m^3)
C_{im} = imaginary gas phase concentration in equilibrium with the adsorbed concentration inside the microparticle (kmol/m^3)
CMSMD = constant surface diffusivity macropore, surface and micropore diffusion
C_0 = characteristic concentration for the fluid concentration (kmol/m^3)
C_μ = adsorbed concentration in the particle (kmol/m^3)
$C_{\mu 0}$ = characteristic concentration for the adsorbed concentration (kmol/m^3)
$C_{\mu,obs}$ = observed adsorbed concentration in the particle (kmol/m^3)
$C_{\mu s}$ = isotherm parameter (kmol/m^3)
D_p = macropore diffusivity (m^2/s)
D_μ = surface diffusivity (m^2/s)
$D_{\mu 0}$ = zero coverage surface diffusivity at infinite temperature in particle coordinate (m^2/s)
E = adsorbate-adsorbent interaction energy (kJ/mol)
e = nondimensional energy defined in Table 1
F = energy distribution function
f = nondimensional energy distribution function defined in Table 1

F_{up} = fractional uptake in Tables 6 and 8
H = function defined in Table 1
HMSMD = heterogeneous macropore, surface and micropore diffusion
J_p = flux through the macropore (kmol/m^2/s)
J_μ = flux through the solid (kmol/m^2/s)
k_m = film mass-transfer coefficient (m/s)
MSMD = macropore, surface and micropore diffusion
r = particle radial position (m)
R = particle radius (m) or gas constant (kJ/kmol/K)
r_μ = position within the microparticle (m)
R_μ = diffusion length in the microparticle direction (m)
R_μ/β = effective diffusion length in the microparticle direction (m)
s = geometric factor of particle (=0, 1, 2 for slab, cylinder and sphere respectively) or isotherm parameter in Unilan isotherm equation
s_μ = geometric factor of microparticle (=0, 1, 2 for slab, cylinder and sphere respectively)
T = temperature (K)
t = real-time (s)
x = nondimensional particle radial position
x_μ = nondimensional microparticle position
Y_b = nondimensional adsorbate concentration in the bulk phase
Y = nondimensional adsorbate concentration in the macropore phase
Y_μ = nondimensional adsorbed concentration in the particle phase

Greek letters

β^2 = ratio of zero coverage surface diffusivity at infinite temperature in the grain direction to that in the particle direction
η = model parameter defined in Table 1
δ = model parameter defined in Table 1
ϵ_M = particle macropore porosity
γ = parameter defined in Table 1
λ = model parameter defined in Table 1
σ = model parameter defined in Table 1
σ_μ = model parameter defined in Table 1
τ = nondimensional time defined in Table 1

Literature Cited

Bhatia, S. K., "Combined Surface and Pore Volume Diffusion in Porous Media," *AIChE J.*, **34**, 1094 (1988).

Do, D. D., "Adsorption in Porous Solids Having Bimodal Pore Size Distribution," *Chem. Eng. Commun.*, **23**, 27 (1983).

Do, D. D., and X. Hu, "An Energy Distributed Model for Adsorption Kinetics in Large Heterogeneous Microporous Particles," *Chem. Eng. Sci.* (in press, 1992).

Do, D. D., X. Hu, and P. L. J. Mayfield, "Multicomponent Adsorption of Ethane, n-Butane and n-Pentane in Activated Carbon," *Gas Separation and Purification*, **5**, 35 (1991).

Do, D. D., and R. G. Rice, "On the Relative Importance of Pore and Surface Diffusion in Non-Equilibrium Adsorption Rate Processes," *Chem. Eng. Sci.*, **42**, 2269 (1987).

Doong, S. J., and R. T. Yang, "Bulk Separation of Multicomponent Gas Mixtures by Pressure Swing Adsorption: Pore/Surface Diffusion and Equilibrium Models," *AIChE J.*, **32**, 397 (1986).

Dubinin, M. M., "On Methods for Estimating Micropore Parameters of Activated Carbons," *Carbon*, **26**, 97 (1988).

Gray, P. G., "Fundamental Studies of Sorption Dynamics of SO_2, NO_2 and CO_2 on Activated Carbon," PhD Thesis, University of Queensland, Australia (1991).

Gray, P. G., and D. D. Do, "Adsorption and Desorption of Gaseous Sorbates on a Bidispersed Particle with Freundlich Isotherm. II. Experimental Study of Sulphur Dioxide Sorption on Activated Carbon Particles," *Gas Separation and Purification*, **3**, 201 (1989).

Gray, P. G., and D. D. Do, "Adsorption and Desorption of Gaseous Sorbates on a Bidispersed Particle with Freundlich Isotherm. III. Contribution of Surface Diffusion to the Sorption Dynamics of Sulphur Dioxide on Activated Carbon," *Gas Separation and Purification*, **4**, 149 (1990).

Horas, J. A., H. A. Saitua, and J. Marchese, "Surface Diffusion of Adsorbed Gases on an Energetically Heterogeneous Porous Solid," *J. Colloid Interface Sci.*, **126**, 421 (1988).

Hu, X., and D. D. Do, "Multicomponent Adsorption Kinetics of Hydrocarbons onto Activated Carbon: Effect of Adsorption Equilibrium Equations," *Chem. Eng. Sci.*, **47**, 1715 (1992a).

Hu, X., and D. D. Do, "Multicomponent Adsorption Kinetics of Hydrocarbons onto Activated Carbon: Contribution of Micropore Resistance," *Chem. Eng. Sci.*, (in press, 1992b).

Kapoor, A., and R. T. Yang, "Surface Diffusion on Energetically Heterogeneous Surfaces," *AIChE J.*, **35**, 1735 (1989).

Kapoor, A., and R. T. Yang, "Surface Diffusion on Energetically Heterogeneous Surfaces—An Effective Medium Approximation Approach," *Chem. Eng. Sci.*, **45**, 3261 (1990).

Kapoor, A., and R. T. Yang, "Contribution of Concentration-Dependent Surface Diffusion to Rate of Adsorption," *Chem. Eng. Sci.*, **46**, 1995 (1991).

Kapoor, A., R. T. Yang, and C. Wong, "Surface Diffusion," *Cat. Rev. Sci. Eng.*, **31**, 129 (1989).

Mayfield, P. L. J., "Fundamental Investigations into Adsorption Kinetics of Light Hydrocarbons onto Activated Carbon," PhD Thesis, University of Queensland, Australia (1990).

Mayfield, P. L. J., and D. D. Do, "Measurement of the Single-Component Adsorption Kinetics of Ethane, Butane and Pentane onto Activated Carbon Using a Differential Adsorption Bed," *Ind. Eng. Chem. Res.*, **30**, 1262 (1991).

Moon, H., and C. Tien, "Adsorption of Gas Mixtures on Adsorbents with Heterogeneous Surfaces," *Chem. Eng. Sci.*, **41**, 2967 (1988).

Myers, A. L., "Adsorption of Pure Gases and Their Mixtures on Heterogeneous Surfaces," in *Fundamentals of Adsorption*, A. L. Myers and G. Belfort, eds., Engineering Foundation, New York, pp. 365-381 (1984).

Petzold, L. R., "A Description of DASSL: A Differential/Algebraic Equation System Solver," *Sandia Technical Report: SAND 82-8637*, Livermore, CA (1982).

Reid, R. C., J. M. Prausnitz, and B. E. Polling, *The Properties of Gases and Liquids*, 4th ed., McGraw-Hill, New York (1987).

Ruthven, D. M., *Principles of Adsorption and Adsorption Processes*, Wiley, New York (1984).

Schneider, P., and J. M. Smith, "Chromatographic Study of Surface Diffusion," *AIChE J.*, **14**, 886 (1968).

Schork, J. M., and J. R. Fair, "Parametric Analysis of Thermal Regeneration of Adsorption Bed," *Ind. Eng. Chem. Res.*, **27**, 457 (1988).

Seidel, A., and P. S. Carl, "The Concentration Dependence of Surface Diffusion for Adsorption on Energetically Heterogeneous Adsorbents," *Chem. Eng. Sci.*, **44**, 189 (1989).

Sun, L. M., and F. Meunier, "A Detailed Model for Non-isothermal Sorption in Porous Adsorbents," *Chem. Eng. Sci.*, **42**, 1585 (1987).

Villadsen, J., and M. L. Michelsen, *Solution of Partial Differential Equation Models by Polynomial Approximation*, Prentice-Hall, Englewood Cliffs, NJ (1978).

Yang, R. T., *Gas Separation by Adsorption Processes*, Butterworth, Boston, MA (1987).

Zgrablich, G., V. Pereyra, M. Ponzi, and J. Marchese, "Connectivity Effects for Surface Diffusion of Adsorbed Gases," *AIChE J.*, **32**, 1158 (1986).

Manuscript received Apr. 21, 1992, and revision received July 28, 1992.